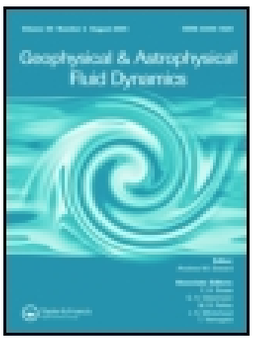

Geophysical & Astrophysical Fluid Dynamics

ISSN: 0309-1929 (Print) 1029-0419 (Online) Journal homepage: http://www.tandfonline.com/loi/ggaf20

The effect of time-dependent γ-pumping on buoyant magnetic structures

Abrar A. Ali & Lara J. Silvers

To cite this article: Abrar A. Ali & Lara J. Silvers (2018): The effect of time-dependent γ-pumping on buoyant magnetic structures, Geophysical & Astrophysical Fluid Dynamics, DOI: 10.1080/03091929.2018.1537396

To link to this article: https://doi.org/10.1080/03091929.2018.1537396

Published online: 26 Oct 2018.

GEOPHYSICAL & ASTROPHYSICAL FLUID DYNAMICS
https://doi.org/10.1080/03091929.2018.1537396

Taylor & Francis
Taylor & Francis Group

The effect of time-dependent γ-pumping on buoyant magnetic structures

Abrar A. Ali and Lara J. Silvers

Department of Mathematics, City University of London, Northampton Square, London, UK

ABSTRACT

In this paper, we explore for the first time the interactions of the net downward, time-dependent, γ-pumping overlying an imposed layer of magnetic fluid, in a polytropic atmosphere. Our calculations show that an equipartition of energy, between the magnetic and kinetic components, must be reached for buoyancy-driven magnetic structures to rise into the pumping region. However, structures do not rise unhindered, as in a previous investigation. We show that the evolution and other features of the emerging magnetic flux structures are significantly affected by the temporal variation of the γ-pumping. The rate of emerging structures, the strength of magnetic concentrations and the extent to how far magnetic field can travel were all found to depend on the timescale of the γ-pumping.

ARTICLE HISTORY
Received 9 May 2018
Accepted 15 October 2018

KEYWORDS
Convection; instabilities; MHD; sun: interior; sun: magnetic fields

1. Introduction

Observed magnetic concentrations in sunspots together with other magnetic phenomena on, and above, the solar surface have given rise to a series of challenging questions regarding the mechanisms responsible for the generation, evolution and escape of magnetic fields from the deep interior to the surface of the Sun (Zwaan 1985; Solanki 2003; Silvers 2008). Consequently, a number of investigations have been undertaken (see e.g. Parker 1993; Dikpati and Gilman 2001; Tobias and Weiss 2007, and references therein) and it is clear that the tachocline region, which is located at the interface of the convection zone and radiative zone, is important as part of both the dynamo mechanism and also in the formation of strong structures that emerge to give rise to features at the surface (see e.g. Spiegel and Zahn 1992; Gilman 2005; Christensen-Dalsgaard and Thompson 2007).

The tachocline is regarded as the seat of large-scale toroidal field in the Sun and is a region of strong shear (Charbonneau 2010). Structures must be formed in this region and remain coherent through the inescapable distortion and shredding in the turbulent convection zone, in order to reach the surface and give rise to magnetic features. A key issue that remains to be understood is how strong structures are formed, and on an appropriate timescale, in the tachocline to give rise to, for example, sunspots at the surface. While a recent investigation has focused on the formation of solar surface magnetic concentrations

CONTACT Abrar A. Ali abrar.ali.1@city.ac.uk

within the convection zone itself (Perri and Brandenburg 2018), a significant body of literature has sought to examine magnetic buoyancy instabilities of a shear-generated magnetic field (see e.g. Cline et al. 2003; Vasil and Brummell 2008; Silvers et al. 2009, and references therein). For simplicity, many of these calculations examine buoyant magnetic tubes in isolation, i.e. in the absence of an overlying convective layer. However, to understand the entire picture of the dynamics, it is important to consider the evolution of magnetic structures in the presence of convection.

Previous numerical papers, looking at the interaction between buoyant magnetic flux structures and convection (Nordlund et al. 1992; Brandenburg et al. 1996; Tobias et al. 1998, 2001), focused on the role of turbulent convection in transporting and storing the underlying magnetic field. In their models, they establish a radial pumping that arises naturally from the turbulent convective flow. However, due to the complex interactions in these frameworks, it is difficult to isolate more general phenomena that permit global features, namely the emergence of magnetic flux tubes, to occur. Few studies have considered the simpler approach of parameterising the pumping effects seen in magnetoconvection simulations using the basis of mean field electrodynamics (Krause and Rädler 1980; Moffatt 1983), to capture such global features (see, for example, Ossendrijver et al. 2002). This so-called γ-pumping simply implies a secondary advection term of the mean magnetic field relative to the flow and can be characterised to describe properties of the turbulent convective flow without the associated complications of full convection calculations (Moffatt 1983; Tobias et al. 2001).

Recently, Barker et al. (2012) implemented the γ-pumping approach in their model to simply capture the dynamics of overshooting convection on buoyant magnetic structures forming in the tachocline. Results from their numerical calculations establish that structures rise from their initial formation region only when an equipartition relation between the magnetic field and the γ-pumping is satisfied. This suggested a plausible mechanism of restraining and intensifying the magnetic field before buoyant structures rise into, and through the convection zone. However, their calculations were an initial limited investigation in this framework as a number of features were not considered and thus may not capture the full picture of the dynamics of the magnetic field in the presence of turbulent convection. Velocities associated with turbulence naturally depend on both time and space (Toomre et al. 1984; Weiss et al. 1996, 2004), and it is unclear how the magnetic field would evolve if the static pumping profile in the (Barker et al. 2012) model was replaced with a time-dependent one. A time-dependent γ-pumping will cause temporal variations in the mean downward force and hence, the equipartition value. The research presented here will build on the work of Barker et al. (2012) by exploring the effect of time-dependent pumping on the formation and evolution of magnetic structures.

This paper will proceed as follows: Section 2 outlines the model, parameter selection and numerical approach. Section 3 discusses the results and this is followed by the conclusions in Section 4.

2. The Model

We consider a localised model in a Cartesian geometry, with x and y corresponding to the horizontal coordinates. The z-axis is chosen to point vertically downwards, parallel to the constant gravitational force, g. In a similar vein to Barker et al. (2012), the fluid is assumed

to obey the perfect gas law with the dynamic viscosity, μ, the magnetic diffusivity, η, the thermal conductivity, κ, and the specific heats at constant density and pressure, c_v and c_p, respectively, all constant. Thus, the set of non-dimensional equations are

$$\frac{\partial \rho}{\partial t} + \boldsymbol{\nabla}\cdot(\rho \boldsymbol{u}) = 0, \tag{1}$$

$$\rho\left(\frac{\partial \boldsymbol{u}}{\partial t} + (\boldsymbol{u}\cdot\boldsymbol{\nabla})\boldsymbol{u}\right) = -\boldsymbol{\nabla} p - \boldsymbol{\nabla}\left(\tfrac{1}{2}F|\boldsymbol{B}|^2\right) + F(\boldsymbol{B}\cdot\boldsymbol{\nabla})\boldsymbol{B} + \sigma C_k(\boldsymbol{\nabla}\cdot\boldsymbol{\tau}) + \rho\theta(m+1)\hat{\boldsymbol{z}}, \tag{2}$$

$$\frac{\rho}{(\gamma_s - 1)}\left(\frac{\partial T}{\partial t} + (\boldsymbol{u}\cdot\boldsymbol{\nabla})T\right) = -p\boldsymbol{\nabla}\cdot\boldsymbol{u} + \frac{\gamma_s C_k}{(\gamma_s - 1)}\boldsymbol{\nabla}\cdot(\kappa\boldsymbol{\nabla}T) + C_k\left(F\zeta_0|\boldsymbol{\nabla}\times\boldsymbol{B}|^2 + \tfrac{1}{2}\sigma\tau^2\right), \tag{3}$$

$$\frac{\partial \boldsymbol{B}}{\partial t} = \boldsymbol{\nabla}\times(\boldsymbol{u}\times\boldsymbol{B} - C_k\zeta_0\boldsymbol{\nabla}\times\boldsymbol{B}) + \boldsymbol{G}, \tag{4}$$

$$\boldsymbol{\nabla}\cdot\boldsymbol{B} = 0, \tag{5}$$

where

$$p = \rho T, \tag{6}$$

and

$$\tau_{ij} = \frac{\partial u_i}{\partial x_j} + \frac{\partial u_j}{\partial x_i} - \frac{2}{3}\frac{\partial u_k}{\partial x_k}\delta_{ij}. \tag{7}$$

Here, ρ is the fluid density, p is the pressure, T is the temperature, $\boldsymbol{B}$ is the magnetic field and $\boldsymbol{u}$ is the fluid velocity. Following notation and scalings in previously related papers (e.g. Matthews et al. 1995b; Silvers et al. 2009), the unit of length is scaled by the depth of the layer, d. Density and temperature are scaled by their initial values at the upper surface, ρ_0 and T_0, respectively, and magnetic field is scaled by the magnitude of the initial magnetic field, B_0. Velocities are scaled by the sound travel-time across the layer in terms of the isothermal sound speed, $\sqrt{(c_p - c_v)T_0}$. In the above equations, $\sigma = \mu c_p/\kappa$ is the Prandtl number, $C_k = \kappa/\rho_0 c_p d\sqrt{(c_p - c_v)T_0}$ is the dimensionless thermal diffusivity, $\zeta_0 = \eta c_p \rho_0/\kappa$ is the ratio of magnetic to thermal diffusivity at the top of the layer, $\gamma_s = c_p/c_v$ is the ratio of specific heats, $\theta = \Delta d/T$ is the temperature gradient, $m = gd/(c_p - c_v)\Delta T - 1$ is the polytropic index and lastly $F = {B_0}^2/(c_p - c_v)T_0\rho_0\mu_0$ is the dimensionless field strength.

As in Barker et al. (2012), the model has been modified to incorporate flux pumping effects via $\boldsymbol{G} = \boldsymbol{\nabla}\times(\boldsymbol{\gamma}\times\boldsymbol{B})$ in (4). It is to be noted that, this modulation of pumping only captures the effect of small-scale turbulence on the evolution of the large-scale magnetic field. Although this mathematical approach does not consider the scales of convection which are comparable or larger than the buoyancy modes, it is to provide an understanding of the underlying physical interactions that influence buoyant magnetic structures.

Unlike in Barker et al. (2012), $\boldsymbol{\gamma}$ will be time-dependent as its derivation incorporates spatial but not temporal averaging (see Moffatt 1983, for a discussion of the form

for $\boldsymbol{\gamma}$). In this paper, the time-dependent, vertical γ-pumping profile is chosen to have the following form

$$\boldsymbol{\gamma} = \gamma(z,t)\hat{\boldsymbol{z}} = \tfrac{1}{2}\gamma_m\left[1+\sin(kt)\right]\left[1+\tanh\left((\Delta z_i)^{-1}(z_i-z)\right)\right]\hat{\boldsymbol{z}}, \tag{8}$$

where k controls the variation of the pumping in time, and where γ is always greater than, or equal to, zero. The spatial dependency of the pumping has been selected to represent the change that occurs between the radiative and convection zones with the pumping gradually decaying to zero at the interface of the two zones. As this is the first inclusion of a time-dependent γ-pumping in such a model, the time-dependent nature of the pumping has been chosen to behave in a simple oscillatory pattern to ease our understanding of the dynamics in a controlled, and well-defined, framework. Figure 1 shows how the γ-pumping varies in space and time for one of the cases that we will discuss in this paper.

In the horizontal directions, the system is assumed to satisfy periodic boundary conditions. The imposed boundary conditions at the top and bottom of the domain are

$$u_z = \frac{\partial u_x}{\partial z} = \frac{\partial u_y}{\partial z} = B_x = B_y = 0, \qquad T = T_0 \qquad \text{at} \qquad z = 0, \tag{9a}$$

$$u_z = \frac{\partial u_x}{\partial z} = \frac{\partial u_y}{\partial z} = B_x = B_y = 0, \qquad \frac{\partial T}{\partial z} = \theta \qquad \text{at} \qquad z = d. \tag{9b}$$

For all calculations, we begin from a state where $\boldsymbol{u} = 0$, $T = T_0(1+\theta z/d)$, $\rho = \rho_0(1+\theta z/d)^m$ and impose a uniform horizontal magnetic layer $\boldsymbol{B} = B_y\hat{\boldsymbol{y}}$, positioned in the region bounded by $z = z_1$ and $z = z_2$ and is zero elsewhere. To accommodate the imposed magnetic field, upon the existing hydrodynamic state, we choose to adjust the density in the magnetic layer so that the system is in equilibrium. Simulations start from this initial state together with small amplitude perturbations of the temperature profile. The equations are solved numerically using a parallel hybrid finite-difference/pseudo-spectral code where time is advanced using a third-order Adams-Bashforth scheme. More detail on the numerical set-up can be found in, for example, Bushby and Houghton (2005).

Table 1 shows the parameter values for our calculations. These are chosen exactly as in Barker et al. (2012) to allow direct comparison with the results of our current investigation

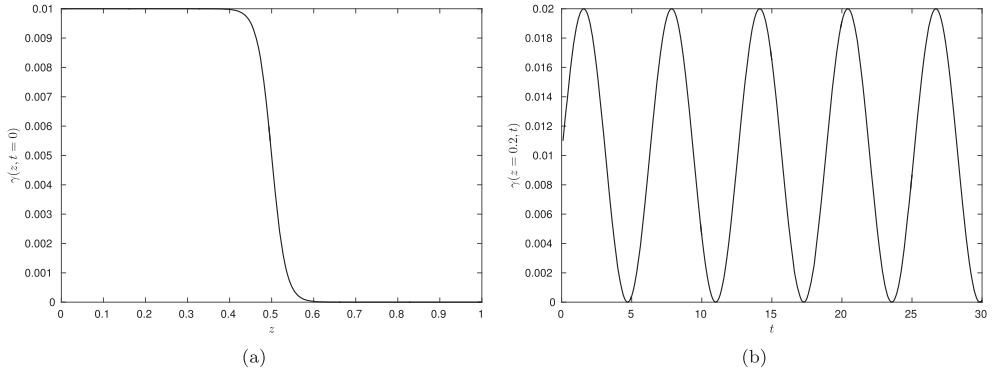

Figure 1. A pumping profile, $\gamma(z,t)$ for $k = 1$, as function of (a) depth at time $t = 0$ and (b) time at depth $z = 0.2$.

Table 1. Parameter values.

Parameter	Description	Value
σ	Prandtl number	0.005
C_k	Thermal diffusivity	0.01
θ	Thermal stratification	2.0
γ_s	Ratio of specific heats	5/3
ζ_0	Magnetic diffusivity	0.01
F	Magnetic field strength	0.01
m	Polytropic Index	1.6
γ_m	Magnetic pumping strength	0.1
z_i	Bottom of pumping layer	0.5
$(\Delta z_i)^{-1}$	Width of transition layer	30.0
z_1, z_2	Top and bottom of magnetic layer	0.6, 0.8
λ_x, λ_y	Box horizontal aspect ratio	1.0, 4.0
d	Vertical depth of box	1.0
$B_y(t=0)$	Initial Horizontal magnetic strength	1.0
k	Frequency associated with magnetic pumping	Variable

when a time-dependent pumping profile is included. The only variable quantity in the present simulations is k. To generally explore the effect of k, on the dynamics of the magnetic field, we initially discuss three cases: Case 1 where $k=1$, Case 2 where $k=0.1$ and Case 3 where $k=0.01$, and thereafter discuss the implications of our general investigation for the Sun. The choice of parameters represent a sub-adiabatic, stratified layer with a computational domain elongated in parallel to the imposed discontinuous field, to allow vortex-induced instabilities and three-dimensional structures to form Matthews et al. (1995a). The γ-pumping is subsonic in order to mimic the magnetic effects resulting from compressible turbulent convection (Tobias et al. 2001). Non-zero diffusion coefficients are incorporated into the system by explicitly defining the diffusive length scales to be considerably larger than the scale of the unresolved convection. As in Barker et al. (2012), these diffusivities should be considered as eddy diffusivities due to the unresolved small-scales of convection, which is consistent with the spirit of the mean field framework.

3. Results

Here we examine the effects of a time-dependent magnetic flux pumping on the results of Barker et al. (2012) by considering a selection of different pumping timescales. In Case 1, the pumping profile is as given in equation (8) where $k=1$, such that the γ-pumping evolves in line with the sound-crossing time. Figure 2 shows snapshots of the magnetic field for this regime. The evolution begins with the uniform magnetic layer embedded in the lower part of the domain (figure 2(a)). As time evolves, an instability occurs leading to the formation of buoyancy-driven magnetic structures rising towards the pumping region (figure 2(b)). Once the magnetic field reaches the base of the γ-pumping region, z_i, magnetic flux concentrations begin to intensify as a result of the competing effect of magnetic buoyancy and γ-pumping below the interface. Locally ascending magnetic structures and descending fluid are known to give rise to three-dimensional arching of the magnetic field (Matthews et al. 1995a), as seen in figure 2(c). Emerging magnetic flux tubes continue to rise in figure 2(d) but are soon pushed back down in figure 2(e). This is in contrast with the earlier findings of Barker et al. (2012), where magnetic structures were observed to rise continually once the magnetic field achieves the equipartition value determined by

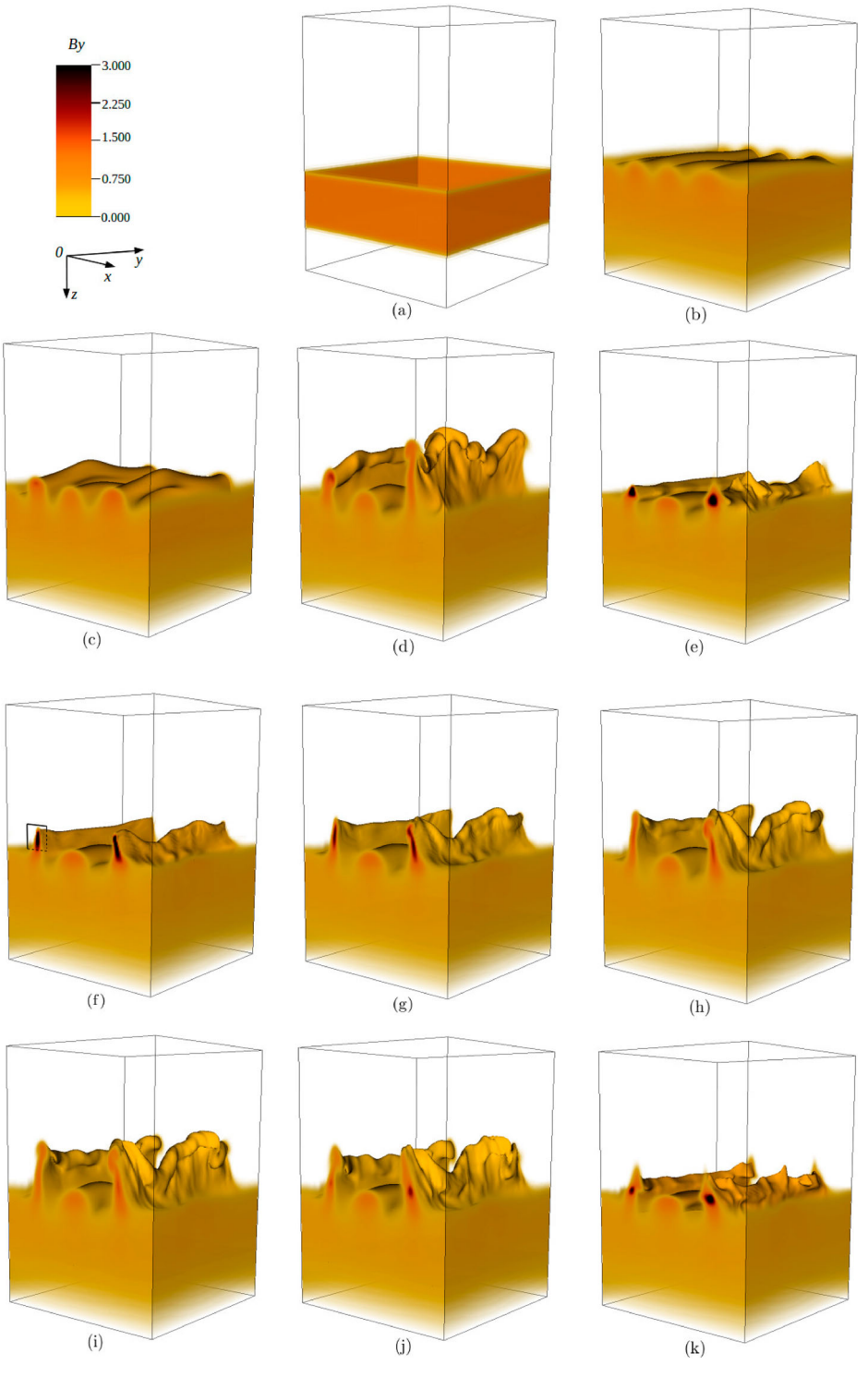

Figure 2. Snapshots of the *y*-component of the magnetic field for Case 1 at (a) $t = 0.69$, (b) $t = 156.8$, (c) $t = 188.5$, (d) $t = 206.5$, (e) $t = 208.6$, (f) $t = 210.8$, (g) $t = 211.5$, (h) $t = 212.2$, (i) $t = 212.9$, (j) $t = 213.6$ and (k) $t = 214.4$, respectively (Colour online).

the Alfvénic Mach number for the γ-pumping at the interface,

$$M_\gamma = (B_y(t))^{-1}\gamma_m\sqrt{\rho(z_i)/F}\,. \tag{10}$$

In our framework, M_γ must be modified to allow for temporal and spatial variations. That is, to take into account the time-dependent nature of the γ-pumping and to determine the action of the magnetic field across various depths, i.e.

$$M_\gamma = (B_y(t))^{-1}\gamma(z,t)\sqrt{\rho(z)/F} = (B_y(t))^{-1}B_{eq}(z,t)\,, \tag{11}$$

where B_{eq} denotes the equipartition value of the mean magnetic field with the γ-pumping.

To analyse the behaviour of emerging magnetic flux in greater detail, we examine the horizontal magnetic component of the field in the y-direction as a function of time and depth. Figure 3 focuses on an individual magnetic flux tube (see the box in figure 2(f) for a visualisation of the region of interest) at the particular point $x = 0.25$ and $y = 0$, and study the changes that are occurring to the magnetic field in relation to the strength of the γ-pumping. In order to enable a clearer interpretation of the results, the difference $B_{eq} - B_y$ is also plotted; positive values of $B_{eq} - B_y$ represent changes in the magnetic field and/or the magnetic flux pumping such that the γ-pumping is able to hold back the upward transport of the magnetic field.

Figure 3(a) shows that, at the near-interface region z_i, the intense magnetic structure is starting to escape the lower layer where $B_{eq} - B_y < 0$. The extent to how far the structure can travel depends on whether an equipartition-strength mean magnetic field is achieved. This magnetic structure continues to rise to the upper layer in figure 3(b,c), while the field generally decreases in magnitude. Eventually, further through the upper domain, the magnetic strength, B_y, becomes insufficient to overcome the threshold equipartition value, and so $B_{eq} - B_y > 0$, where the pumping prevents the magnetic field from rising.

Given the γ-pumping timescale for variation in Case 1, the strength of the pumping and hence the equipartition value begins to increase in figure 3(d). This can be seen in the difference $B_{eq} - B_y$ at the top, i.e. $z < 0.2$, where $B_y \approx 0$. Rising magnetic structures experience the maximum downward force at the upmost depth achieved, due to the nature of the pumping profile. Thus, we observe the amplification of the magnetic field, B_y, just above $z \approx 0.4$, in addition to the field being pushed downwards. This behaviour continues with the growth of the equipartition value, as a result of the increase in the pumping strength, in figure 3(e). Finally, figure 3(f) shows that the γ-pumping achieves sufficient strength to push and maintain the magnetic field below $z \approx 0.5$, in addition to the intensification of the magnetic field.

We find in Case 1 that magnetic structures are regularly pushed down and repelled back up due to the temporal variation of the magnetic pumping. There is found to be a dependency on the parameter M_γ, that controls the ascent of localised magnetic structures. In the phase $M_\gamma \gtrsim 1$, i.e. $B_{eq} - B_y > 0$, magnetic field is found to be held down with strong concentrations generated below the interface. Transitioning to $M_\gamma \lesssim 1$, these concentrations become sufficiently stronger than the present equipartition threshold. Hence, rising to the upper domain until the periodic pumping cycle reaches high levels of strength, returning background magnetic field to the lower layer. The pumping layer, occupying the region

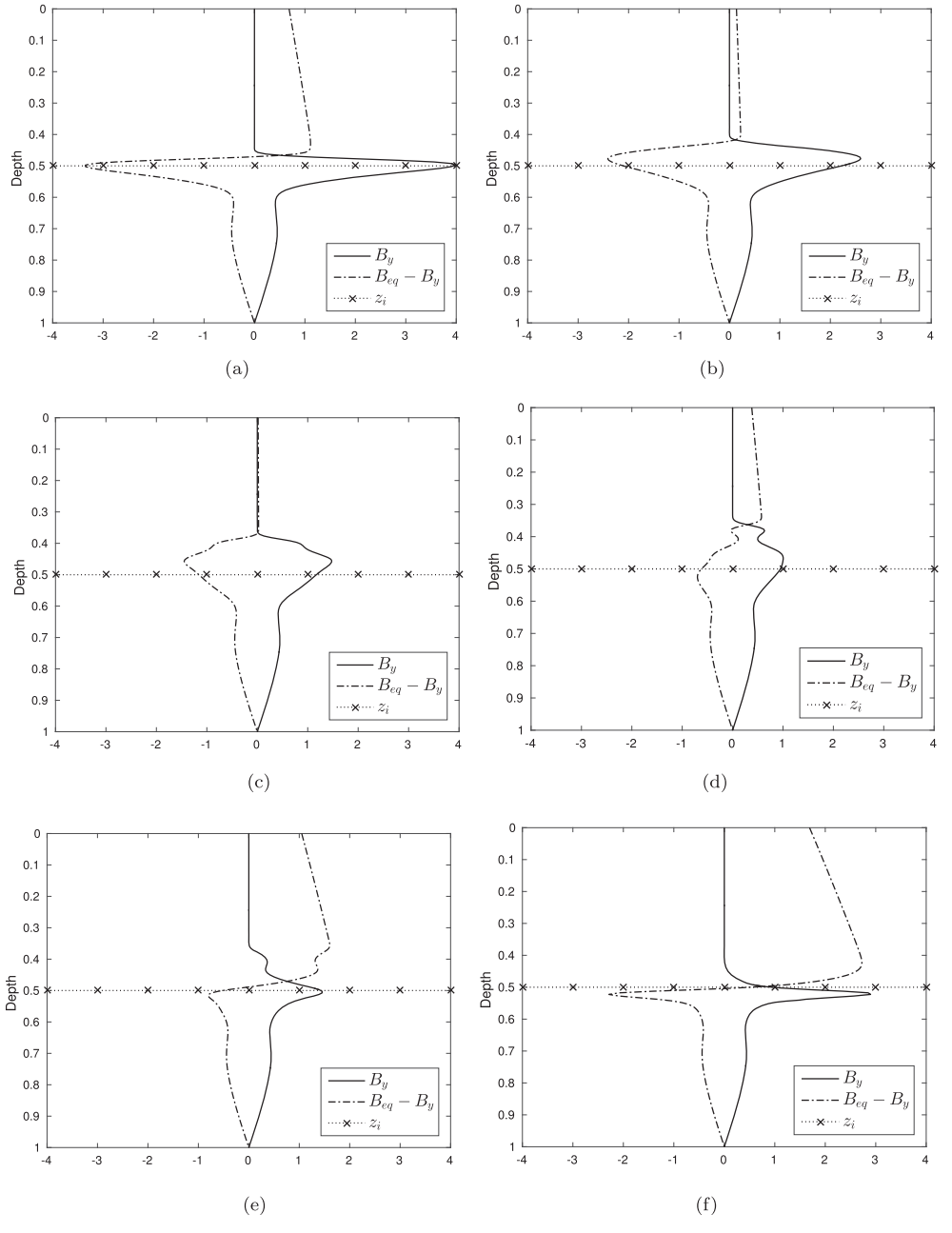

Figure 3. The horizontal magnetic field B_y and $B_{eq} - B_y$ vs. depth for a magnetic structure in Case 1, located at $x = 0.25$ and $y = 0$, at times (a) $t = 210.8$, (b) $t = 211.5$, (c) $t = 212.2$, (d) $t = 212.9$, (e) $t = 213.6$ and (f) $t = 214.4$.

above z_i, acts as a filter permitting magnetic structures to rise through the upper layer once the desired strength is attained while maintaining the storage of the magnetic field at the lower layer. Nevertheless, variations in the pumping timescale play a key role in the emergence of magnetic structures.

To explore the behaviour of emerging magnetic structures further, we reduce the frequency of the pumping cycle by setting $k = 0.1$. For this case (Case 2), we find the spreading of the initial field consistent with Case 1. Once the magnetic field has diffused and reached the pumping zone, the contribution of different pumping timescales can become evident.

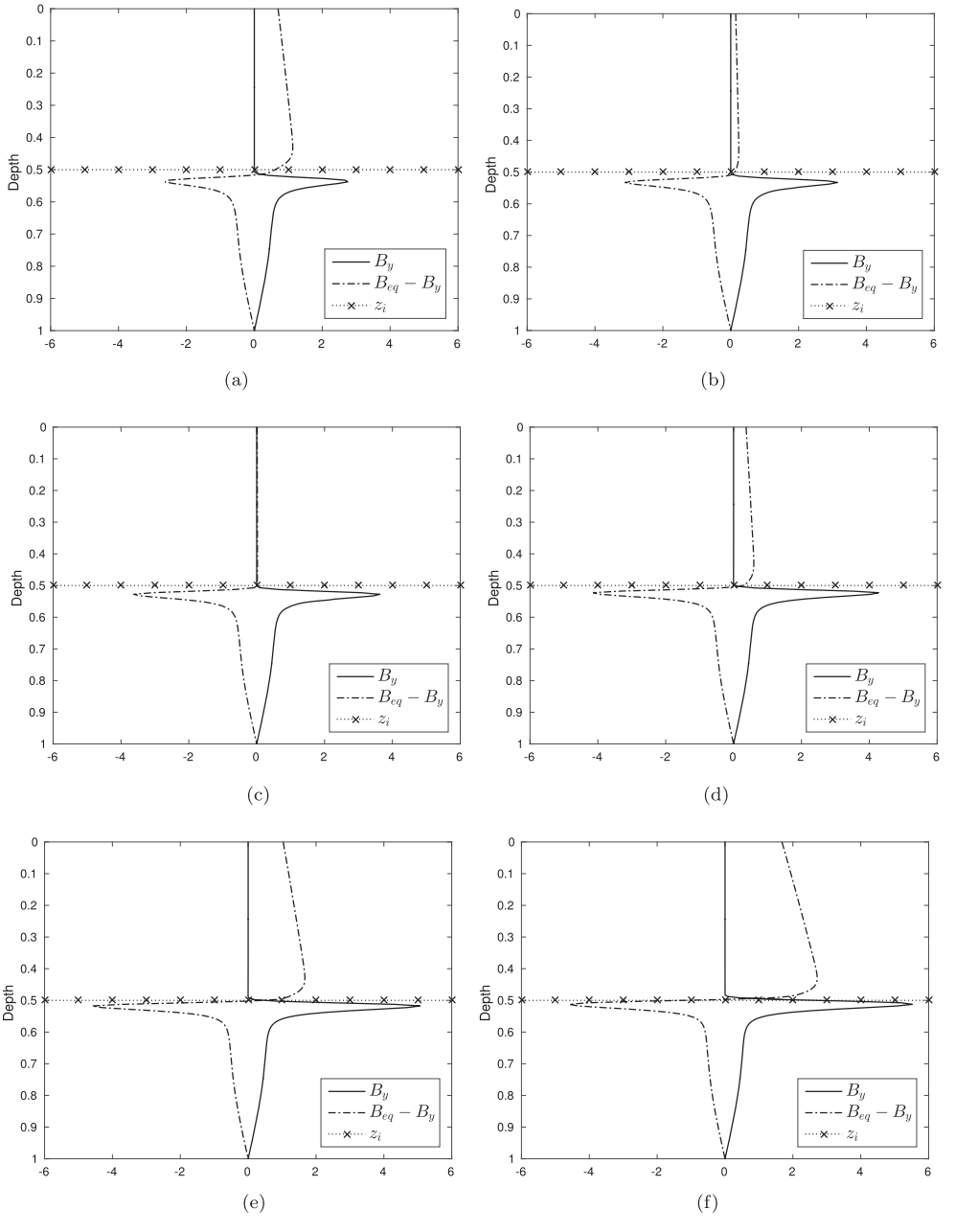

Figure 4. The horizontal magnetic field B_y and $B_{eq} - B_y$ vs. depth for a magnetic structure in Case 2, located at $x = 0.25$ and $y = 0$, at times (a) $t = 210.8$, (b) $t = 211.5$, (c) $t = 212.2$, (d) $t = 212.9$, (e) $t = 213.6$ and (f) $t = 214.4$.

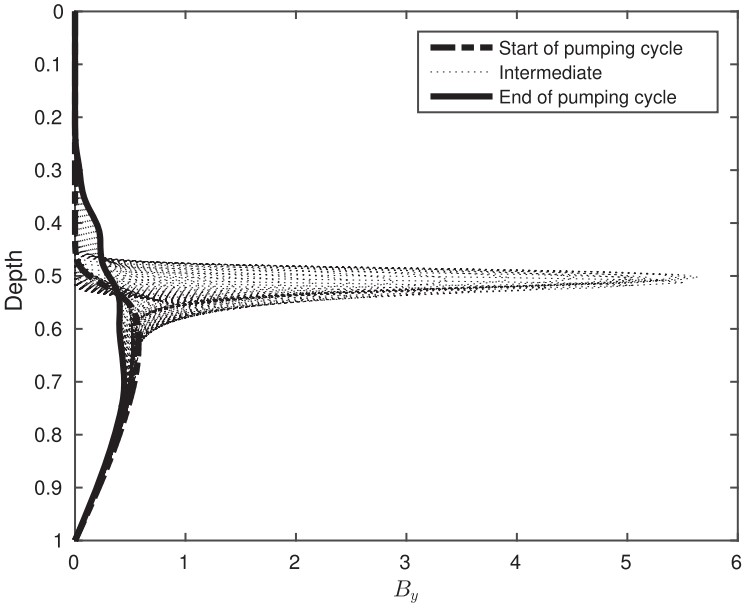

Figure 5. B_y vs. depth, for a magnetic structure in Case 2, located at $x = 0.25$ and $y = 0$, at regularly-spaced time intervals. The pumping cycle starts at $t = 171.9$ and ends at $t = 236.8$.

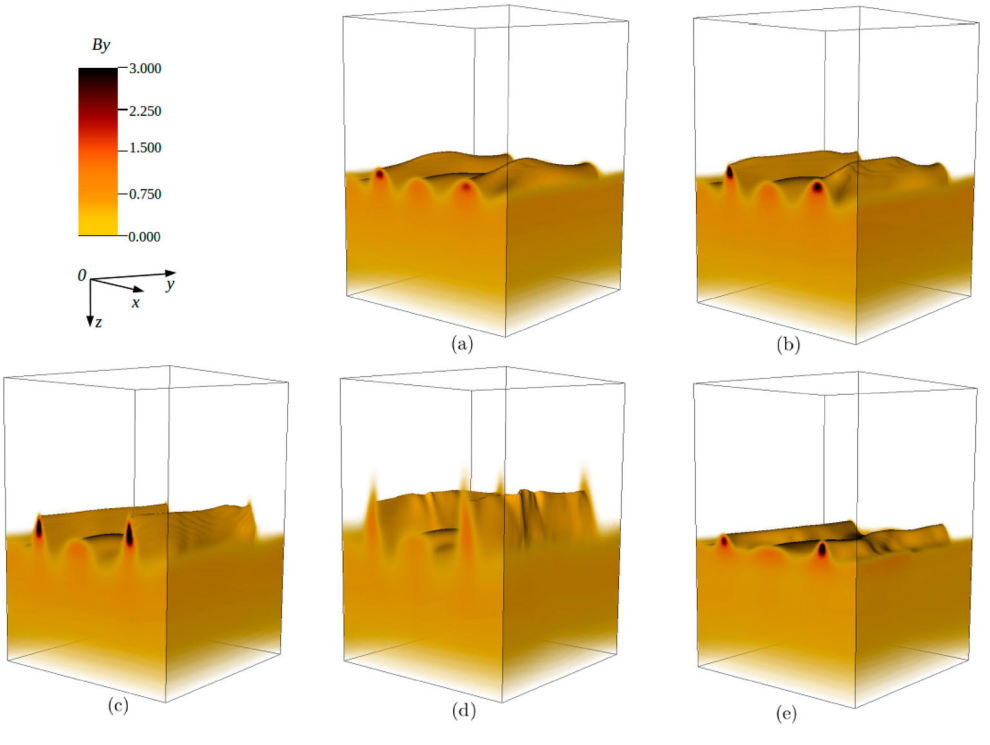

Figure 6. Snapshots of the y-component of the magnetic field for Case 2 at (a) $t = 210.8$, (b) $t = 214.4$, (c) $t = 222.3$, (d) $t = 233.9$ and (e) $t = 254.8$, respectively (Colour online).

To compare Case 2 with Case 1, figure 4 shows the evolution of a magnetic structure located at $x = 0.25$ and $y = 0$ for a period of time, similar to that in figure 3.

In contrast with Case 1, figure 4(a,b) shows that the emergence of a magnetic structure is delayed to a later stage. This is a result of the pumping strength varying at a slower

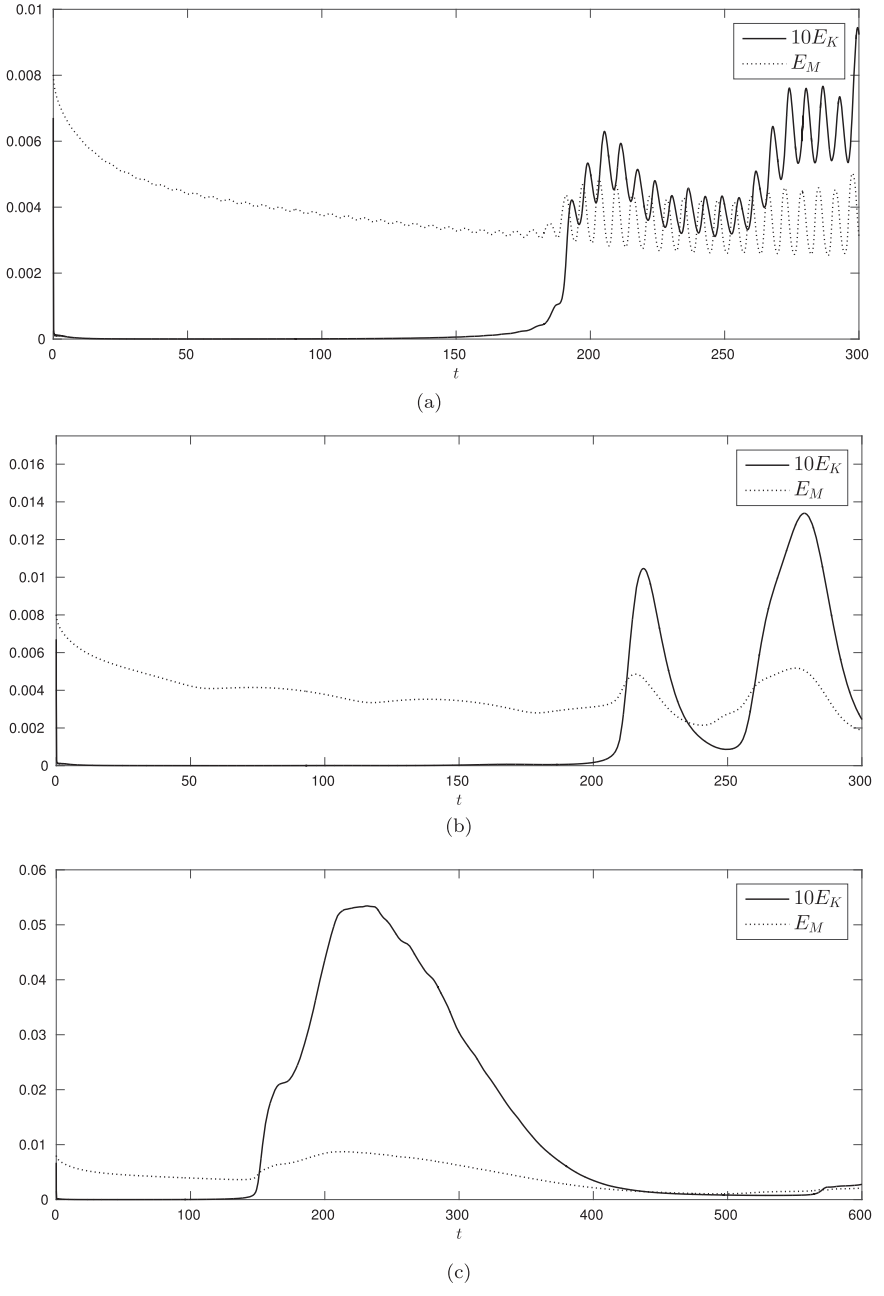

Figure 7. Temporal evolution of the total kinetic energy and magnetic energy for (a) Case 1, (b) Case 2 and (c) Case 3. Note that Case 3 is shown for a longer period than Cases 1 and 2 to consider a complete pumping cycle.

pace in Case 2. Consequently, the interactions between the γ-pumping and magnetic field occur over a longer timescale, leading to the generation of stronger magnetic concentrations below $z \approx 0.5$ as shown in figure 4(c–f). Within the time period where we have clear magnetic emergence in Case 1, for Case 2 the magnetic equipartition value is always dominant in the upper domain. Therefore, no flux emergence is observed and so it is useful to explore the magnetic emergence across a broader time range.

Figure 5 elaborates on the evolution of the particular magnetic structure considered in figure 4, during one complete pumping cycle. Magnetic flux emergence is consistent with the equipartition criteria established earlier. However, we notice that the magnetic field spreads further throughout the pumping region. This is because, for slower temporal variation in the γ-pumping, magnetic concentrations are able to travel further once emergence takes place. Additionally, at particular stages, the pumping strength decays, followed by the equipartition value. Hence, allowing the buoyancy-driven magnetic structure to rise. Snapshots of the nonlinear evolution of the horizontal magnetic field in Case 2 are shown in figure 6.

Evolution of the total kinetic and magnetic energies for Case 1, Case 2 and an additional Case 3, where $k = 0.01$, are shown in figure 7. The growth of the kinetic and magnetic energies arise from the mechanisms responsible for the enhancement of the local magnetic field. This is followed by the almost periodic release of energies, depending on the imposed pumping profile, leading to the emergence of magnetic concentrations into the upper region of our domain. For Case 1, magnetic structures rise frequently, but with weaker strengths in comparison to Case 2 and Case 3. The intensification process of magnetic field in Case 3 is more effective, due to the pumping strength varying over a longer timescale, hence allowing the magnetic field to interact efficiently with the γ-pumping.

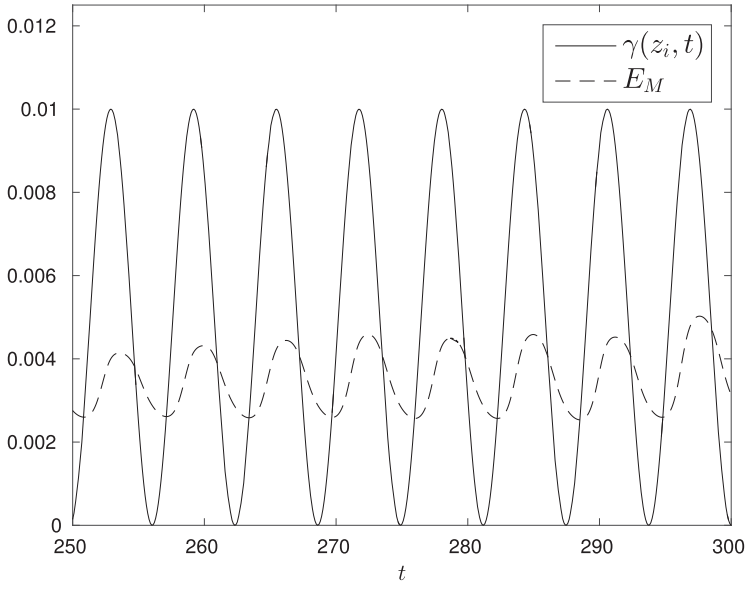

Figure 8. Comparison between the variation of the imposed pumping profile and magnetic energy for Case 1.

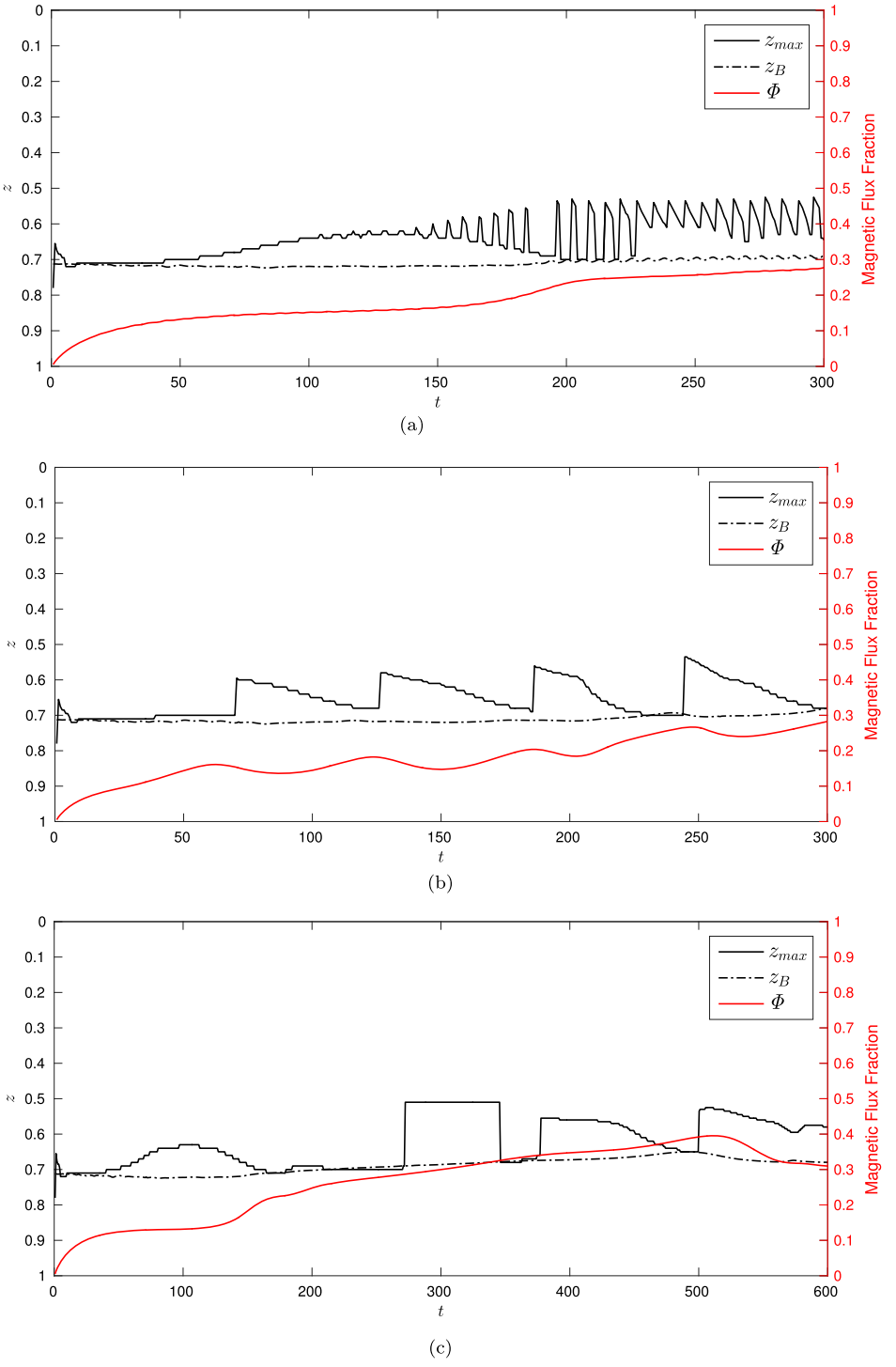

Figure 9. The location of the maximum magnetic field, $z_{\max}$, location of centre of magnetic field, z_B, and the magnetic flux fraction contained above the initial location of magnetic field, Φ, in time, for (a) Case 1, (b) Case 2 and (c) Case 3 (Colour online).

The action of buoyant magnetic structures shows a correlation with the temporal variation of the γ-pumping. This is displayed in figure 8 by comparing a γ-profile evolution with its associated magnetic energy for Case 1. Pumping peaks are shown to be in agreement with the generation of the strongest magnetic field strength at each cycle of the turbulent pumping profile. To examine further the differences in the three cases, we apply standard measures of depth with respect to the maximum value and centre of the magnetic field (Wissink et al. 2000; Tobias et al. 2001). These quantities are given by

$$z_{\max} = z \Big| \max_z \langle B_y \rangle (z), \tag{12}$$

$$z_B = \int_0^1 z \langle B_y \rangle \, \mathrm{d}z \Big/ \int_0^1 \langle B_y \rangle \, \mathrm{d}z, \tag{13}$$

respectively, where $\langle B_y \rangle = \iint B_y \ \mathrm{d}x\mathrm{d}y$. Additionally, we quantify the fraction of magnetic flux present in the part of the domain above the initial location of the magnetic field,

$$\Phi = \int_0^{0.6} \langle B_y \rangle \, \mathrm{d}z \Big/ \int_0^1 \langle B_y \rangle \, \mathrm{d}z \,. \tag{14}$$

Figure 9 shows $z_{\max}$, z_B, and Φ versus time for Cases 1–3. Generally, an initial decline in $z_{\max}$ is observed as the magnetic field is subject to diffusion. This is shortly recovered by the magnetic buoyant force, causing magnetic fields to rise within the lower region of our computational domain. Interactions between magnetic buoyancy and magnetic pumping become more effective, after $t \approx 50$, once the redistribution of the magnetic flux reaches the interface region. This competition persists along with the formation of magnetic concentrations, near z_i.

The depth to which maximal magnetic concentrations are attained, $z_{\max}$, in time vary based on the particular choice of k. In Case 3, for example, since the pumping evolves slowly, the intensification and breakout of the field occurs on a longer timescale. The dynamics is more varied for Case 1, where local field amplification occurs more frequently. In all cases, the bulk of the field is maintained at the lower fraction of the domain, as shown by the global measure z_B. The measure Φ highlights the general effect of the γ-pumping on the spread of the magnetic field above where it is initially located. The fraction of magnetic flux is shown to be greater for Case 3, reaching approximately 40% of the total initial flux, which indicates that magnetic structures are able to spread further for slower temporal variations in the γ-pumping.

4. Conclusions

We have examined how the time-dependent γ-pumping impacts on the formation and evolution of buoyant structures using an idealised mathematical framework. All simulations began with an initial state, thermally perturbed, giving rise to buoyant magnetic structures at the surface of the discontinuous magnetic layer. As in the earlier work of Barker et al. (2012), the bulk of the magnetic field was found to be maintained below the interface in all cases with only locally intense concentrations of magnetic flux rising against the γ-pumping, i.e. only structures where the magnetic field strength is comparable to equipartition strength. However, we found that in all of our cases, the time-dependent

nature of the γ-pumping profile gave rise to a more complex evolution to what was seen in Barker et al. (2012), where structures continue to rise once the equipartition threshold was achieved. In the cases we considered, magnetic structures were found to rise into the upper half of the domain but, as time progressed, were then pushed back down towards the lower domain. This behaviour is a result of the competing effects of buoyant magnetic structures and downward, time-dependent pumping velocity.

To understand the effect of time-dependent γ-pumping, we considered three different pumping timescales. Properties including the rate of emergence, strength and spread of magnetic field were all found to depend on the characteristics of the γ-pumping profile. The degree of flux emergence was found to correlate with the frequency of the imposed magnetic pumping. Further, the intensity of magnetic structures was found to vary as the pumping timescale varied. Emerging structures obtained higher magnetic strength and travelled further into the pumping layer when slower temporal variations in the pumping profile were imposed.

In our model, we sought to focus on the general effect of time-dependent pumping, on the action of rising magnetic structures. However, based on theoretically derived timescale estimates of convection turnover, Kim and Demarque (1996) expressed two different convective timescales: a global, large-scale, convective turnover time for the complete convection zone and a local, smaller-scale, convective turnover time near the base of the convection zone. Approximate measurements of the local solar convective timescale, in terms of the variable k, fall within $k < 0.001$. This is not easily accessible in our current model framework. However, by gradually decreasing the value of k, we were able to extract meaningful patterns of the rising magnetic structures. Additionally, our simplified model assumes a regular periodicity in the pumping, which is unlikely to occur in the Sun, but it does show that the evolution of buoyant structures is very dependent on changes to the convection. Structures of sufficient strength, relative to the downward motions, will rise and can reach the solar surface. Weaker structures will be halted in the ascent and then will interact with the turbulence, forming part of the interface dynamo model.

Finally, while this mathematical model was principally constructed to help understand interactions that occur near the base of the solar convection zone, the solar photospheric layer also displays variation in the timescale of convective motions as well as in the scales of emerging magnetic flux through, for instance, granulation patterns (Priest 2014). Therefore, the work here also gives a little insight into the dynamics of convective turbulence and emergence of magnetic structures in the photospheric region. The γ-pumping we considered with the fastest time variation showed frequent rise of relatively weak, compared to the other cases considered, magnetic structures. This is clearly not the situation deep in the convection zone, but it is very likely in the near surface region of the Sun, where granular magnetic loops are observed to appear very frequently in small magnetic concentrations. Further commentary on the dynamics of both the solar surface region and deep interior are to be considered via a more complex model.

Acknowledgements

The computations were performed using the solon supercomputer at City, University of London and the Cambridge Service for Data Driven Discovery (CSD3) operated by the University of Cambridge Research Computing Service (www.csd3.cam.ac.uk). The authors thank the anonymous reviewers

for their valuable suggestions and comments and are grateful to Benjamin Favier and Veronika Witzke for their helpful discussions throughout this work.

Disclosure statement

No potential conflict of interest was reported by the authors.

Funding

This research has been financially supported by the Science and Technology Facilities Council (STFC) studentship award [grant number ST/M503459/1]. The use of Cambridge Service for Data Driven Discovery (CSD3) at the University of Cambridge was provided by Dell EMC and Intel using Tier-2 funding from the Engineering and Physical Sciences Research Council [grant number EP/P020259/1], and DiRAC funding from the Science and Technology Facilities Council (www.dirac.ac.uk).

References

Barker, A.J., Silvers, L.J., Proctor, M.R.E. and Weiss, N.O., Magnetic buoyancy instabilities in the presence of magnetic flux pumping at the base of the solar convection zone. *Mon. Not. Roy. Astron. Soc.* 2012, **424**, 115–127.

Brandenburg, A., Jennings, R.L., Stein, R.F. and Tuominen, I., Magnetic structures in a dynamo simulation. *J. Fluid Mech.* 1996, **306**, 325–352.

Bushby, P.J. and Houghton, S.M., Spatially intermittent fields in photospheric magnetoconvection. *Mon. Not. Roy. Astron. Soc.* 2005, **362**, 313–320.

Charbonneau, P., Dynamo Models of the Solar Cycle. *Living Rev. Sol. Phys.* 2010, **7**, 3–91.

Christensen-Dalsgaard, J. and Thompson, M., Observational results and issues concerning the tachocline. In *The Solar Tachocline*, edited by D.W. Hughes, R. Rosner and N.O. Weiss, pp. 53–85, 2007 (Cambridge Univ. Press: Cambridge).

Cline, K.S., Brummell, N.H. and Cattaneo, F., On the formation of magnetic structures by the combined action of velocity shear and magnetic buoyancy. *Astron. Astrophys.* 2003, **588**, 630–644.

Dikpati, M. and Gilman, P.A., Flux-transport dynamos with α effect from global instability of tachocline differential rotation: a solution for magnetic parity selection in the Sun. *Astrophys. J.* 2001, **559**, 428–442.

Gilman, P.A., The tachocline and the solar dynamo. *Astron. Nachr.* 2005, **326**, 208–217.

Kim, Y.-C. and Demarque, P., The theoretical calculation of the Rossby number and the "non-local" convective overturn time for pre–main-sequence and early post–main-sequence stars. *Astrophys. J.* 1996, **457**, 340–347.

Krause, F. and Rädler, K.-H., *Mean Field Magnetohydrodynamics and Dynamo Theory*, 1980 (Pergamon Press: Oxford).

Matthews, P.C., Hughes, D.W. and Proctor, M.R.E., Magnetic buoyancy, vorticity, and three-dimensional flux-tube formation. *Astrophys. J.* 1995a, **448**, 938–941.

Matthews, P.C., Proctor, M.R.E. and Weiss, N.O., Compressible magnetoconvection in three dimensions: planforms and nonlinear behaviour. *J. Fluid Mech.* 1995b, **305**, 281–305.

Moffatt, H.K., Transport effects associated with turbulence with particular attention to the influence of helicity. *Rep. Prog. Phys.* 1983, **46**, 621–664.

Nordlund, Å., Brandenburg, A., Jennings, R.L., Rieutord, M., Ruokolainen, J. and Stein, R.F., Dynamo action in stratified convection with overshoot. *Astrophys. J.* 1992, **392**, 647–652.

Ossendrijver, M., Stix, M., Brandenburg, A. and Rüdiger, G., Magnetoconvection and dynamo coefficients: II. Field-direction dependent pumping of magnetic field. *Astron. Astrophys.* 2002, **394**, 735–746.

Parker, E.N., A solar dynamo surface wave at the interface between convection and non-uniform rotation. *Astrophys. J.* 1993, **408**, 707–719.

Perri, B. and Brandenburg, A., Spontaneous flux concentrations from the negative effective magnetic pressure instability beneath a radiative stellar surface. *Astron. Astrophys.* 2018, **609**, A99.
Priest, E., *Magnetohydrodynamics of the Sun*, 2014 (Cambridge Univ. Press: Cambridge).
Silvers, L.J., Magnetic fields in astrophysical objects. *Philos. T. Roy. Soc.* 2008, **366**, 4453–4464.
Silvers, L.J., Bushby, P.J. and Proctor, M.R.E., Interactions between magnetohydrodynamic shear instabilities and convective flows in the solar interior. *Mon. Not. Roy. Astron. Soc.* 2009, **400**, 337–345.
Solanki, S.K., Sunspots: an overview. *Astron. Astrophys. Rev.* 2003, **11**, 153–286.
Spiegel, E.A. and Zahn, J.-P., The solar tachocline. *Astron. Astrophys.* 1992, **265**, 106–114.
Tobias, S.M., Brummell, N.H., Clune, T.L. and Toomre, J., Pumping of magnetic fields by turbulent penetrative convection. *Astrophys. J.* 1998, **502**, L177–L180.
Tobias, S.M., Brummell, N.H., Clune, T.L. and Toomre, J., Transport and storage of magnetic field by overshooting turbulent compressible convection. *Astrophys. J.* 2001, **549**, 1183–1203.
Tobias, S.M. and Weiss, N.O., The solar dynamo and the tachocline. In *The Solar Tachocline*, edited by D.W. Hughes, R. Rosner and N.O. Weiss, pp. 319–350, 2007 (Cambridge Univ. Press: Cambridge).
Toomre, J., Hurlburt, N.E. and Massaguer, J.M., Strong downward plumes resulting from compressibility in nonlinear convection and their coupling to gravity waves. In *Small-scale dynamical processes in quiet stellar atmospheres*, edited by S. Kiel, pp. 222–234, 1984 (Sunspot: National Solar Observatory).
Vasil, G.M. and Brummell, N.H., Magnetic buoyancy instabilities of a shear-generated magnetic layer. *Astrophys. J.* 2008, **686**, 709–730.
Weiss, N.O., Brownjohn, D.P., Matthews, P.C. and Proctor, M.R.E., Photospheric convection in strong magnetic fields. *Mon. Not. Roy. Astron. Soc.* 1996, **283**, 1153–1164.
Weiss, N.O., Thomas, J.H., Brummell, N.H. and Tobias, S.M., The origin of penumbral structure in sunspots: downward pumping of magnetic flux. *Astrophys. J.* 2004, **600**, 1073–1090.
Wissink, J.G., Hughes, D.W., Matthews, P.C. and Proctor, M.R.E., The three-dimensional breakup of a magnetic layer. *Mon. Not. Roy. Astron. Soc.* 2000, **318**, 501–510.
Zwaan, C., The emergence of magnetic flux. *Sol. Phys.* 1985, **100**, 397–414.